文章编号: 1001 - 9014(2018)06 - 0693 - 06

DOI:10.11972/j.issn.1001 - 9014.2018.06.010

Study on the electric field modulation effect of ultrathin alumina layer

XU Da-Peng, CHENG Pei-Hong, CHEN Lin*, ZHANG David Wei

(State Key Laboratory of ASIC and System, School of Microelectronics, Fudan University, Shanghai 200433, China)

Abstract: The characteristics and mechanism of set/reset process in high-k based resistive random-access memory devices were studied. A great fluctuation in set/reset voltages was observed in the NbAlO single-layer RRAM devices. However, it shows highly uniform and reproducible switching cycles in Al_2O_3/NbAlO/Al_2O_3 nanolaminate stack structures. Based on the electric-filed modulating effect, we proposed a unified resistive switching model to simulate the set and reset operations, and the switch parameters dispersion due to the great randomness of the conductive spots formation or annihilation was discussed for a single-layer RRAM. When an ultra-thin Al_2O_3 films was embedded in NbAlO-based RRAM devices, there is an obvious improvement in the stabilization of the set/reset switching voltages. It can be explained that the electric-field distribution is rearranged and locally controlled in the stack structure, therefore the conductive filament bridges and ruptures appear in the thin buffer layer.

Key words: electric-filed modulating effect, resistive random access memory (RRAM), atomic layer deposition

PACS: 77.55.D-, 74.40.-n, 73.40.Rw

超薄氧化铝层的电场调制效应

徐大朋, 程佩红, 陈 琳*, 张 卫

(复旦大学 微电子学院 专用集成电路与系统国家重点实验室,上海 200433)

摘要:研究了基于高k介质材料的阻变存储器的写入/擦除(SET/RESET)特性和物理机制. 研究发现基于NbAlO材料的阻变存储器SET/RESET电压具有较大波动性,通过结构优化,在Al_2O_3/NbAlO/Al_2O_3纳米薄片堆垛结构器件中获得高度稳定性的可重复的阻变特性. 基于电场调制效应,提出了一种统一的电阻开关模型去模拟阻变存储器的SET/RESET行为,并探讨了单层阻变薄膜的阻变存储器中由导电单元形成和湮灭的巨大随机性引起的阻变特性分布. 当在NbAlO基阻变存储器中嵌入超薄Al_2O_3膜后,阻变存储器的SET/RESET电压稳定性将显著提升,其原因在于采用堆垛结构的阻变器件中各介质层中的电场重新分布并精确可控,因此导电细丝的导通/断裂通过电场调制作用稳定均匀地在发生在具有高电场的薄缓冲层介质层中.

关 键 词:电场调制; 阻变存储器; 原子层沉积

中图分类号:TN30 **文献标识码**:A

Introduction

As traditional flash memory is now facing a dimension limit, an emergent emerging of the investigation has been carried out on the resistive switching phenomena for potential application in the next generation of memory devices, naming resistive random access memory (RRAM)[1-9]. The resistive switching memory system offers superior scalability since its simple structure means that only one dimension should be critically controlled. However, issues such as the set and reset voltage dispersion and the unstable resistance states profile has hampered the development of RRAM[10-15]. Many experimental results have been reported for the commercialization of RRAM cells, but there have been only a small number of modeling researches and the fundamental physical mechanism is still not clear[16-21].

Received date: 2018-04-03, **revised date**: 2018-08-24 **收稿日期**:2018-04-03, **修回日期**:2018-08-24

Foundation items:Supported by National Natural Science Foundation of China (61376092, 61076114, 61106108, 51172046), Specialized Research Fund for the Doctoral Program of Higher Education (20110071130005)

Biography:XU Da-Peng (1984-), male, Shandong, China, PhD. Research area involves Semiconductor materials and devices. E-mail:16110720080@fudan.edu.cn. CHENG Pei-Hong, contributed equally to this work

* **Corresponding author**:E-mail:linchen@fudan.edu.cn

Generally, RRAM modeling is classified into two categories: the microscopic and macroscopic descriptions. The former explains RRAM switching mechanism in an atomic level[22-23]. Although useful for the accurate prediction of material property, it is not suitable for the simulation of real RRAM cells or array because it consumes a large amount of computational resources. Moreover, mechanism of RRAM operation could not be understood completely through the microscopic descriptions. Accordingly, macroscopic descriptions, advantageous in modeling of real cells and array, have attracted much attention. However, although some pioneering macroscopic RRAM models have been proposed, their applicability to experimental data is still limited. The most widely used random circuit breaker (RCB) network model[24-26] can simulate only two-dimensional structures and orthogonal-direction current flow. For thermal modeling, it is not accurate for reset operation. Though Russo et al. proposed a more accurate model for reset operation[27-28], it cannot simulate RRAM cells with the CFs generated by forming or set operation, even assuming that conductive filament (CF) is predefined.

In this work, a unified resistive switching model has been proposed for the accurate prediction of forming, reset, and set operations, and the effect of electric field modulating (EFM) to the dispersion of set and reset voltages will also be discussed. Various resistive switching stacks are used in the RRAM structure instead of a single layer. Based on the facts of the different conductivities and dielectric constants between the different dielectric films, the electrical field can be rearranged and locally controlled in the stack structure.

1 Experiments

Two groups of NbAlO and ZnO based high-k RRAM devices with or without ultra-thin Al_2O_3 layer were fabricated using atomic layer deposition (ALD) on 100-nm-thick evaporated Pt/SiO_2/Si substrate to form metal-insulator-metal (MIM) structure, as shown in Fig. 1. Here we use $Zn(C_2H_5)_2$, $Al(CH_3)_3$, $Nb(OC_2H_5)_5$ liquid source as metal precursors and H_2O as an oxidant in a hot-wall ALD reactor (ASM F120) at a base pressure of 1 mBar, Nitrogen was used as a carrier and purge gas supplied via a mass flow controller, and the substrate temperature is about 300 and 150 °C, respectively. The NbAlO high-k films were prepared by modulating ALD deposition cycles for Al_2O_3 and Nb_2O_5, and the cycle ratio was set to 3∶1. Subsequently, a diameter of 100 μm TiN top electrode was fabricated by physical vapor sputtering through a lift-off process. Electrical characteristics of the RRAM devices were obtained using Keithley 4200-SCS semiconductor parameter analyzer, with biased on top electrode and grounded on bottom electrode at room temperature.

2 Results

Bipolar switching phenomena can be observed in all RRAM devices under DC voltage sweep, which means that the process for setting the device to ON state occurs at one polarity and the process for resetting to OFF state occurs at the reversed polarity. It can be seen by the current-voltage (*I-V*) characteristics curves in Fig. 2. By sweeping the external positive voltage from zero to a certain voltage, an abrupt increase of current was observed and the low resistance state (LRS) was achieved, and this is defined as the SET operation. Here a compliance current (5 or 10 mA) is set to avoid dielectric hard breakdown. Subsequently, by sweeping from zero to negative, the resistance is abruptly increased at a certain negative voltage, which means that the sample is switched to a high resistance state (HRS), defined as the RESET operation. The LRS and HRS states are stable and can be used as the binary states for memory applications. But the switching voltages of the NbAlO and ZnO single layer RRAM devices, as shown in Figs. 2(a) and (d), were not stably fixed at certain values during continuous switching cycles. The fluctuation in set and reset voltage may be the most serious concern for the real application of resistive switching memory devices.

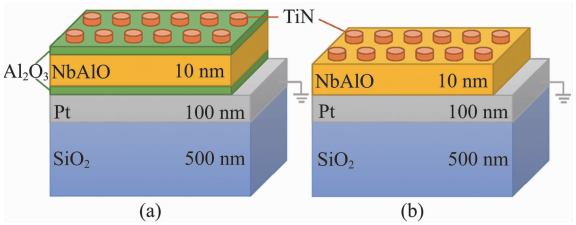

Fig. 1 Structural representation of high-k based RRAM devices (a) with and (b) without Al_2O_3 buffer layers

图1 基于高k介质材料的阻变存储器结构示意图(a)有氧化铝缓冲层的器件,(b)没有氧化铝缓冲层的器件

Then we fabricated TiN/Al_2O_3/high-k/Al_2O_3/Pt nanolaminate stack RRAM structures in order to improve this fluctuation, and the corresponding *I-V* curves were shown in Figs. 2(b) and (e). For TiN/Al_2O_3/NbAlO/Al_2O_3/Pt structure, shown in Fig. 1(a), the set and reset voltage is about 0.8 and −0.8 V, respectively. Statistical measurements and descriptions of the set and reset voltage distributions of all samples were carried out by 100 repeated resistive switch cycles in different cells, as shown in Fig. 2(c). Compared with the TiN/NbAlO/Pt cell, the NbAlO with ultra-thin Al_2O_3 cell presents a great improvement with a much smaller fluctuation in set and reset process, a rather smaller dispersion set/reset voltages were found, along with the highly uniform repeatability set and reset process and the mean values and standard deviation of set/reset voltage ($<V_{set}>$, σV_{set}, $<V_{reset}>$ and σV_{reset}) are 1.09, 0.10, −0.92 and 0.202 V, respectively. However, Figs. 2(d) and (e) exhibit that there is still fluctuation in set and reset voltages for the ZnO-based RRAM devices with and without Al_2O_3 buffer layer, and the statistics data are displayed in Fig. 2(f).

The fluctuation problems in switching devices require clearly understanding of physical origin for switching phenomena. To date, it is widely accepted that the electrons hopping among localized oxygen vacancy under external electric field play a key role in the filamentary conducting mechanism. Although recent random circuit

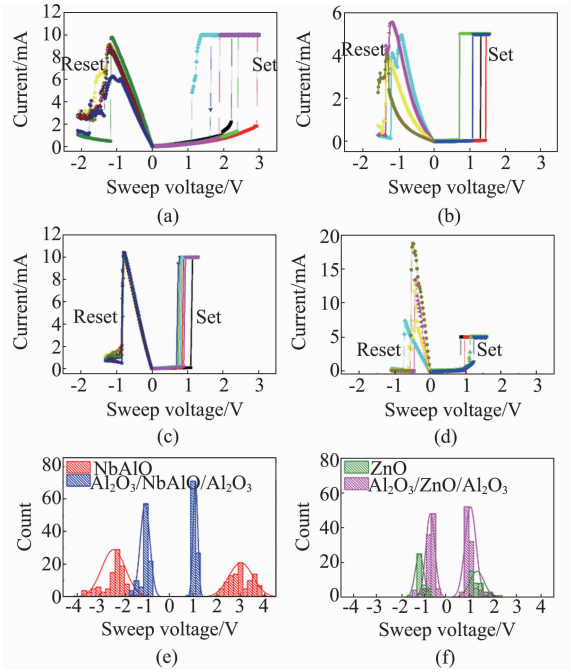

Fig. 2　Bipolar resistive switching phenomena were observed in the *I-V* characteristics for the TiN/Al_2O_3/high-k/Al_2O_3/Pt and TiN/high-k/Pt samples under dc voltage sweep at room temperature, the voltage bias was scanned form 0 to V_{max}, and then from 0 to $-V_{max}$. (a) A quite larger switching voltage dispersion of the set and reset processes in the TiN/NbAlO/Pt cell than, (b) the data in the TiN/Al_2O_3/NbAlO/Al_2O_3/Pt structure, and (c) a rather smaller dispersion values and the highly uniform repetitive in set an reset processes were observed in the stack structure than the sinlge one. But for the ZnO-based RRAM devices with and without buffer layers, there is no obvious difference between, (d) TiN/ZnO/Pt and (e) TiN/Al_2O_3/ZnO/Al_2O_3/Pt, and (f) shows the same normal analyses of the V_{set} and V_{reset} distribution for both ZnO RRAM structures

图 2　在室温下对 TiN/Al_2O_3/high-k/Al_2O_3/Pt 和 TiN/high-k/Pt 结构器件施加直流电压扫描，偏压首先从 0 增加到 V_{max}，然后减小到 0，获得双极性电阻转变特性（a）TiN/NbAlO/Pt 结构器件中写入和擦除电压的波动性明显大于，(b) TiN/Al_2O_3/NbAlO/Al_2O_3/Pt 结构器件，(c) 为 NbAlO 基 RRAM 写入与擦除电压的统计结果，Al_2O_3/NbAlO/Al_2O_3 堆栈结构可以有效减小写入与擦除电压的波动。但对 ZnO 基 RRAM，加入缓冲层对器件性能并未发现明显的改善，(d) TiN/ZnO/Pt 结构，(e) TiN/Al_2O_3/ZnO/Al_2O_3/Pt 堆栈结构，(f) ZnO 基 RRAM 写入与擦除电压的统计

breaker (RCB) network model delineates resistive switch mechanism and explains the large variation in set and reset voltages, it does not illustrate how to minimize the operation voltage randomness. Based on the facts that the different dielectric constant of the dielectric films can induce different electric field dispersion in stack structure, the Al_2O_3/high-k/Al_2O_3 resistive stack were utilized to enhance electrical field in few-nanometer-thick Al_2O_3 layer near electrode. As a result, the formation and rupture of conductive filament is designed to occur within the thin Al_2O_3 region, which the thickness is controlled to be about 2 ~ 3 nm, so the set and reset voltages can be limited into a very narrow range to avoid the universal random formation and rupture problems in a single resistive layer.

3　Discussions

To elucidate the conductive filaments formation and rupture microscopic process in Al_2O_3/high-k/Al_2O_3 resistive switch stack structures, we proposed electrical modulating resistive switch model based on the finite difference method, and then explain why the memory switching parameters dispersion could be minimized by stabilizing the conductive spots generation and annihilation occur location. In our model, an Al_2O_3/NbAlO/Al_2O_3 stack films and a single NbAlO layer RRAM structure has been simulated in comparison with experiment, as shown in Fig. 1, the active area is 0.01 μm^2, and the total dielectric films thickness is 0.02 μm.

In the first place, the cell is divided into small conductive spots, and a fraction of oxygen vacancy is randomly generated on the nodes in the pristine state, here we thought that the vacancy probability near the anode is larger than the other places. Then the electrical potential V and temperature T at each node are solved by Poisson and Fourier heat flow equations when an external voltage V_g is applied[28-29],

$$\nabla(\sigma \nabla V) = 0 \quad , \quad (1)$$

$$-\nabla(\kappa \nabla V) = J^2/\sigma \quad . \quad (2)$$

Here we adopt Dirichlet boundary conditions that $V = V_g$ at the top electrode and $V = 0$ at the bottom electrode, in which each spots conductivity σ depends on the position, $\sigma = \sigma_{CF}$ inside the conductive filaments, and $\sigma = \sigma_{ox}$ in the host material, σ_{CF} is the Mott's hopping conductance and is far greater than material itself. J is the Joule power density and κ is the material thermal conductivity. We assume that the thermal equilibrium is much faster than voltage variations and electrodes act as ideal thermal sinks, which yields $T = T_0$ as the boundary condition.

In our model, each conductive node generation or annihilation probability is governed by local electric field and Joule heating together[30],

$$D = D_0 e^{-(E_A - E)/k_B T} \quad , \quad (3)$$

where E represents local electric field, E_A is an activation energy and k_B is the Boltzmann constant and D_0 is the attempt frequency which we fix to a typical value of atomistic processes, 1.2×10^{12}/s.

Thirdly, when the external voltage is ramped up, a series of conductive spots (oxygen vacancy) are continuously generated according to the calculated probability values at each node, until a conductive filament is formed between the top and bottom electrodes, i. e. the forming process is completed. After that when a reverse bias is applied on the structure, some conductive spots are annihilated due to probability function until CF is disconnected, i. e. the reset process is finished. Then the set operation begins as a positive bias applied again, which is analogous to the forming process. Moreover,

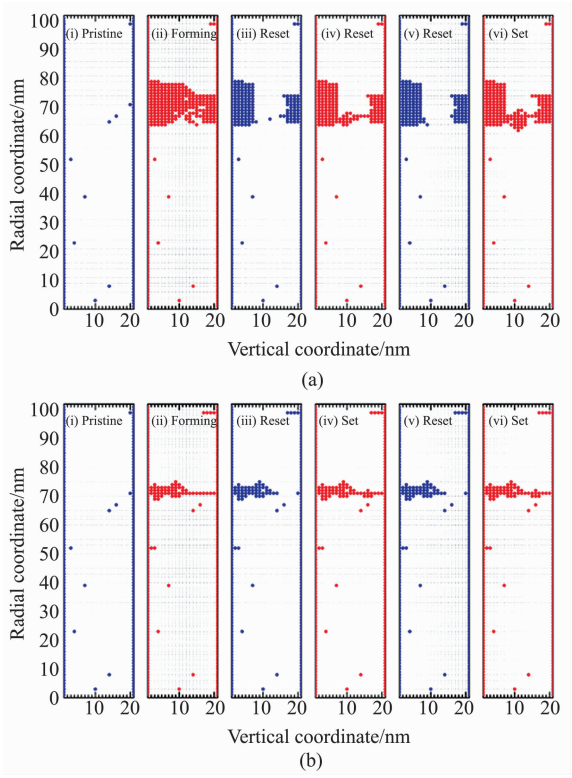

Fig. 3 Resistance switching mechanism for (a) a NbAlO single-layer RRAM devices and (b) a Al_2O_3/NbAlO/Al_2O_3 stack RRAM structure in single-bit operation. Here, (i) Pristine state with a certain vacancy oxygen distribition, (ii) conductive spots generated by probability function until a filament is formed, (iii) the spots state after the first reset process, (iv) post-set, (v) reset and (vi) set state

图3 对不同结构 RRAM，通过模拟得到的单比特操作下电阻转变模型.（a）基于 NbAlO 单层膜的 RRAM，（b）基于 Al_2O_3/NbAlO/Al_2O_3 堆积结构的 RRAM. 其中，(i) 存在一定氧空位的初始状态，(ii) 导电点按照概率函数的形式产生直到导电细丝形成，(iii) 首次擦除 (iv) 随后写入 (v) 再擦除 (vi) 接着写入后的分别得到状态

current between the two electrodes is calculated by using the current continuity equation, and aforementioned reset-set operation cycle (steps # 3 and 4) is repeated. All the parameters used in our model is displayed is the Table 1.

Table 1 Values of the relevant physical parameters used in the electro thermal simulations

表 1 电热模拟中的相关物理参数值

	d_{ox}/nm	σ_{ox}/(S/cm)	σ_{CF}/(S/cm)	κ_{ox}/(W/cm·K)	E_A/eV
Al_2O_3	3, 4	0.1	5 000	1.25 (1 – 10)	1.2
NbAlO	14, 16, 20	0.25	12 500	2.0 (1 – 10)	1.125
ZnO	10, 16	0.125	3 000	1.5(1 – 10)	1.1

The conductive spots and filaments distribution for the NbAlO (20 nm) single-layer and Al_2O_3 (2 nm)/NbAlO (16 nm)/Al_2O_3 (2 nm) stack films RRAM devices are exhibited Fig. 3 (a) and (b), respectively. The electric-field distribution relatively uniform for the single-layer structure, and the conductive spots locations generated according to Eq. (3) are very random in the forming process, which mainly depended on the pristine state. The conductive filaments shape appears relatively uniform size, and the temperature peak due to Joule-heated effect arise at anyplace, therefore the conductive filament rapture location reveals a random distribution.

However, the relative dielectric constant of Al_2O_3 films by ALD is about 7, only about one fifth of Nb_2O_5 (50) for the stack structure, so the electric-field strength in Al_2O_3 thin films is much larger than that in the high dielectric constant (NbAlO) layer. The conductive spots are sparser when closer to the anode after the forming operation, and the filaments shape become thinner and weaker. From Eqs. 1-2, we can see that the conductive spots location and filaments shape have a great impact to E and T in the reset process, its distribution displayed in Fig. 4 when the conductive filament disrupted. Through comparison between the inset figure (iii) in Fig. 3 (b) and Fig. 4, we may also found that the field strength E always gets the maximum value at the most sparse area of the conductive spots, and the temperature T also achieves the largest value in the weakest-link conductive filaments.

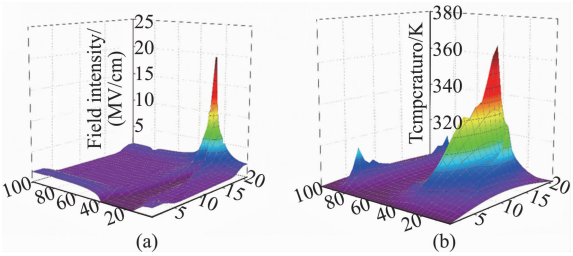

Fig. 4 Calculated (a) electric field intensity and (b) temperature map in a Al_2O_3/NbAlO/Al_2O_3 stack RRAM structures when a reset voltage of −1.35 V on anode. Both the maximum field strength and temperature peak are located in the Al_2O_3 buffer layer close to the top electrode, where the conductive filament is weakest

图4 对 Al_2O_3/NbAlO/Al_2O_3 堆积结构 RRAM，正极施加 −1.35 V 擦除电压时，计算得到（a）电场强度，（b）温度的面分布图。其中，最大电场强度和最高温度均出现在靠近顶电极的氧化铝缓冲层中，因为在这个位置导电细丝最弱

Figure 5 exhibits the simulated I-V characteristics for the for NbAlO-based RRAM devices with and without Al_2O_3 buffer layers, including forming, reset and set process, and the statistical description of the calculated memory switching parameters. The set/reset voltages for a single-layer RRAM structure fluctuate depending on probability function, and its simulated I-V curves exhibited in Fig. 5 (a) conform with experimental data as shown in Fig. 2 (a) in a statistical manner. Simulated average value and standard deviation of set and reset voltage are 1.97, 0.54, −0.78 and −0.09 V, respectively. It should be noted that V_{set} shows wider distribution than V_{reset} because the effective volume where conductive spots are generated or annihilated is different in each case. In the case of reset operation, only a narrow

CF is related to the annihilation of conductive spots. However, in the case of set operation, every partially disconnected conductive filament can contribute to the generation of conductive spots. To sum up, V_{set} is more widely distributed than V_{reset} because more diverse cases can occur in the set operation than in the reset operation[29].

The computational *I-V* curves remain unchanged after the forming and first reset operation for a stack RRAM structure, as shown in Fig. 5 (b), i. e. the operation voltages' randomness is improved. And it can be explained that during set and reset process, the electric-field distribution is modulated due to the different dielectric constant of each layer. As a result, the highest vacancy oxygen generation or annihilation probability will appear in the thin Al_2O_3 film close to the anode according the probability function, and it can greatly reduce the randomness of the switching position and the conductive filaments shape. So we can conclude that the dispersion of the switching parameter could be minimized by stabilizing the spots in the thin Al_2O_3 buffer layer near the anode where conductive filament bridges and ruptures in the cells.

However, there is no improvement in the stabilization of the switching characteristics after the thin Al_2O_3 films embedded for ZnO-based RRAM devices, as shown in Fig. 6. It may be due to minor difference between the dielectric constants of ZnO and Al_2O_3 layer, and the electric field modulation has no effect on this ZnO stack structure. So the conductive spots and filament formation or annihilation appeared great randomness, and the statistical results of the set/reset voltages show no obvious differences with the single ZnO layer RRAM devices, as shown in Fig. 1 (b).

4 Conclusions

In summary, utilizing resistive switch stacks in the RRAM structure instead of a single resistive switching functional layer, the electrical performance can be greatly enhanced. We observed that the embedded thin Al_2O_3 layers could improve bipolar resistive switching characteristics. An electrical field modulating resistive switching model was proposed to give an effective method for minimizing the dispersion of the resistive switching randomness. The electric field modulation model provides an indication of how to optimize the switching parameters such as set/reset voltages dispersion, which is currently considered the most serious obstacle to practical RRAM applications.

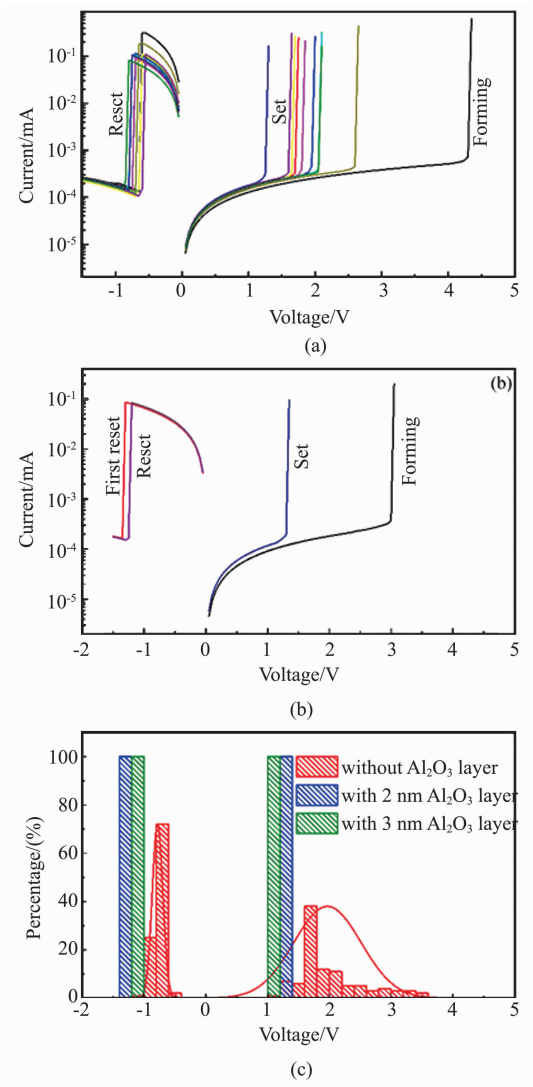

Fig. 5　Simulated *I-V* characteristics curves of the NbAlO-based RRAM structures (a) with and (b) without Al_2O_3 buffer layers after ten set/reset switch cycles. (c) Simulated V_{reset} and V_{set} distribution of NbAlO-based RRAM devices after 100 repeated endurance cycles. A great dispersion in the set/reset voltage values were found in a single NbAlO RRAM cells; but in stack structure with 2 or 3 nm Al_2O_3 ultra-thin films, the switch voltages were fixed at some certain value

图 5　模拟得到的 NbAlO 基 RRAM，在 10 个周期的写入/擦除中电流—电压特性曲线，(a) 有 (b) 没有氧化铝缓冲层. (c) 为使用不同的缓冲层厚度时模拟得到 100 个循环中写入/擦除电压分布。不使用缓冲层时写入/擦除电压存在较大的离散性，而对于存在 2 或 3 nm 超薄氧化铝的堆积结构，开关电压固定在一定值

References

[1] Szot K, Speier W, Bihlmayer G, *et al*. Switching the electrical resistance of individual dislocations in single-crystalline $SrTiO_3$ [J]. *Nat. Mater.* 2006, **5**(4): 312 - 320.

[2] Waser R, Aono M. Nanoionics-based resistive switching memories [J]. *Nat. Mater.* 2007, **6**(11): 833 - 840.

[3] Sawa A, Resistive switching in transition metal oxides [J]. *Materials Today* 2008, **11**(6): 28 - 36.

[4] Waser R, Dittmann R, Staikov G, *et al*. Redox-based resistive switching memories-nanoionic mechanisms, prospects, and challenges [J]. *Adv. Mater.* 2009, **21**(25-26): 2632 - 2663.

[5] Chen L, Xu Y, Sun Q Q, *et al*. Highly uniform bipolar resistive switching with Al_2O_3 buffer layer in robust NbAlO-Based RRAM [J]. *IEEE Electron Dev. Lett.* 2010, **31**(4): 356 - 358.

[6] Yu S, Wu Y, Wong H S P. Investigating the switching dynamics and multilevel capability of bipolar metal oxide resistive switching memory [J]. *Appl. Phys. Lett.* 2011, **98**(10): 103514 - 103516.

[7] Tsai T M, Chang K C, Chang T C, *et al*. Dehydroxyl effect of Sn-doped silicon oxide resistance random access memory with supercritical

CO_2 fluid treatment [J]. *Appl. Phys. Lett.* 2012, **101**(11): 112906-112904.
[8] Salaoru I, Prodromakis T, Khiat A, *et al.* Resistive switching of oxygen enhanced TiO_2 thin-film devices [J]. *Appl. Phys. Lett.* 2013, **102**(1):013506-013504.
[9] Tian B B, Wang J L, Fusil S, *et al.* Tunnel electroresistance through organic ferroelectrics [J]. *Nat. Commun.* 2016, **7**:11502.
[10] Fujimoto M, Koyama H. TiO_2 anatase nanolayer on TiN thin film exhibiting high-speed bipolar resistive switching [J]. *Appl. Phys. Lett.* 2006, **89**(22):223509-223511.
[11] Kim K M, Choi B J, Hwang C S. Localized switching mechanism in resistive switching of atomic-layer-deposited TiO_2 thin films [J]. *Appl. Phys. Lett.* 2007, **90**(24): 242906-242908.
[12] Kim K M, Choi B J, Shin Y C, *et al.* Anode-interface localized filamentary mechanism in resistive switching of TiO_2 thin films [J]. *Appl. Phys. Lett.* 2007, **91**(1):012907-012909.
[13] Gao B, Sun B, Zhang H, *et al.* Unified physical model of bipolar oxide-based resistive switching memory [J]. *IEEE Electron Dev. Lett.* 2009, **30**(12):1326-1328.
[14] Lee M H, Kim K M, Kim G H, *et al.* Study on the electrical conduction mechanism of bipolar resistive switching TiO_2 thin films using impedance spectroscopy [J]. *Appl. Phys. Lett.* 2010, **96**(15):2909-2911.
[15] Zhang H, Gao B, Sun B, *et al.* Ionic doping effect in ZrO_2 resistive switching memory [J]. *Appl. Phys. Lett.* 2010, **96**(12):123502-123504.
[16] Dong R, Xiang W F, Lee D S, *et al.* Improvement of reproducible hysteresis and resistive switching in metal-$La_0.7Ca_0.3MnO_3$-metal heterostructures by oxygen annealing [J]. *Appl. Phys. Lett.* 2007, **90**(18): 182118-182120.
[17] Lin C Y, Lin M H, Wu M C, *et al.* Improvement of resistive switching characteristics in $SrZrO_3$ thin films with embedded Cr layer [J]. *IEEE Electron Dev. Lett.* 2008, **29**(10):1108-1111.
[18] Yin M, Zhou P, Lv H B, *et al.* Improvement of resistive switching in Cu_xO using new RESET mode [J]. *IEEE Electron Dev. Lett.* 2008, **29**(7): 681-683.
[19] Lv H, Wang M, Wan H, *et al.* Endurance enhancement of Cu-oxide based resistive switching memory with Al top electrode [J]. *Appl. Phys. Lett.* 2009, **94**(21):213502-213503.
[20] Choi S J, Kim J H, Lee H H. Deep-UV curing of poly (4-vinyl phenol) gate dielectric for hysteresis-free organic thin-film transistors [J]. *IEEE Electron Dev. Lett.* 2009, **30**(5):454-456.
[21] Shang D S, Shi L, Sun J R, *et al.* Improvement of reproducible resistance switching in polycrystalline tungsten oxide films by in situ oxygen annealing [J]. *Appl. Phys. Lett.* 2010, **96**(7):072103-072105.
[22] Cagli C, Nardi F, Ielmini D. Modeling of set/reset operations in NiO-based resistive-switching memory devices [J]. *IEEE T Electron Dev.* 2009, **56**(8):1712-1720.
[23] Guan X, Yu S, Philip Wong H S. On the switching parameter variation of metal-oxide RRAM - Part I: Physical modeling and simulation methodology [J]. *IEEE T Electron Dev.* 2012, **59**(4):1172-1182.
[24] Chae S C, Lee J S, Kim S, *et al.* Random circuit breaker network model for unipolar resistance switching [J]. *Adv. Mater.* 2008, **20**(6):1154-1159.
[25] Chang S H, Lee J S, Chae S C, *et al.* Occurrence of both unipolar memory and threshold resistance switching in a NiO film [J]. *Phys. Rev. Lett.* 2009, **102**(2):026801.
[26] Lee S B, Yoo H K, Kim K, *et al.* Forming mechanism of the bipolar resistance switching in double-layer memristive nanodevices [J]. *Nanotechnology* 2012, **23**(31):315202.
[27] Russo U, Ielmini D, Cagli C, *et al.* Filament conduction and reset mechanism in NiO-based resistive-switching memory (RRAM) devices [J]. *IEEE T Electron Dev.* 2009, **56**(2):186-192.
[28] Russo U, Ielmini D, Cagli C, *et al.* Self-accelerated thermal dissolution model for reset programming in unipolar resistive-switching memory (RRAM) devices [J]. *IEEE T Electron Dev.* 2009, **56**(2): 193-200.
[29] Lee K, Jang J S, Kwon Y, *et al.* A unified model for unipolar resistive random access memory [J]. *Appl. Phys. Lett.* 2012, **100**(8): 083509-083511.
[30] Li D, Li M, Zahid F, *et al.* Oxygen vacancy filament formation in TiO_2: A kinetic Monte Carlo study [J]. *J. Appl. Phys.* 2012, **112**(7):073512-073517.